Nanoelectronics and Its New Materials – A NEW ERA OF NANOSCIENCE

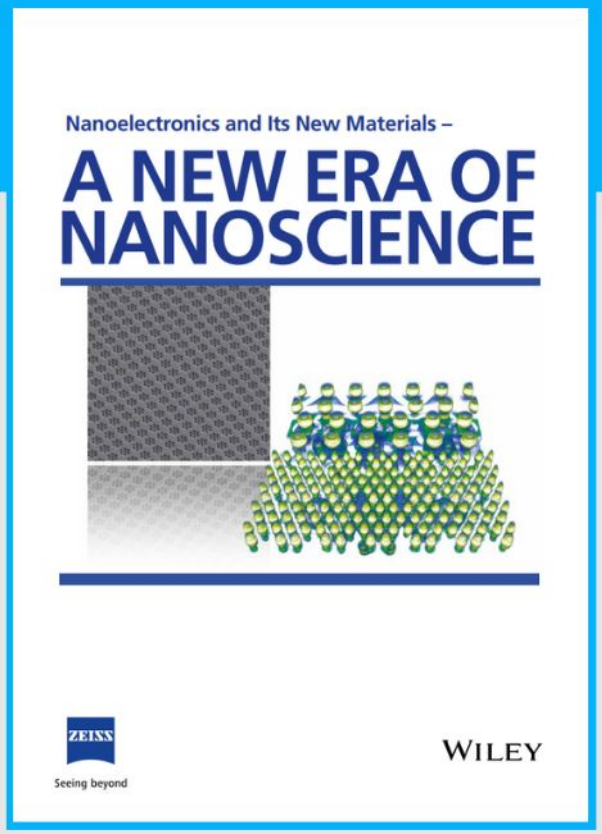

Discover the recent advances in electronics research and fundamental nanoscience.

Nanotechnology has become the driving force behind breakthroughs in engineering, materials science, physics, chemistry, and biological sciences. In this compendium, we delve into a wide range of novel applications that highlight recent advances in electronics research and fundamental nanoscience. From surface analysis and defect detection to tailored optical functionality and transparent nanowire electrodes, this eBook covers key topics that will revolutionize the future of electronics.

To get your hands on this valuable resource and unleash the power of nanotechnology, simply download the eBook now. Stay ahead of the curve and embrace the future of electronics with nanoscience as your guide.

ZEISS

Seeing beyond

WILEY

ADVANCED FUNCTIONAL MATERIALS
www.afm-journal.de

Incommensurate Magnetic Order in Hole-Doped Infinite-Layer Nickelate Superconductors due to Competing Magnetic Interactions

Yajun Zhang, Xu He, Jingtong Zhang, Jie Wang, and Philippe Ghosez*

The discovery of superconductivity in hole-doped infinite-layer nickelates has fueled intense research to identify the critical factor responsible for high-T_c superconductivity. Magnetism and superconductivity are closely entangled, and elucidating the magnetic interactions in hole-doped nickelates is critical for understanding the pairing mechanism. Here, these calculations based on the generalized Bloch theorem (GBT) and magnetic force theorem (MFT) consistently reveal that hole doping stabilizes an incommensurate (IC) spin state and increases the IC wave vector continuously, in a way strikingly similar to hole-doped cuprates. Going further, a nonlinear Heisenberg model including first-neighbor and third-neighbor in-plane magnetic interactions is developed. The analytical solutions successfully reproduce GBT and MFT results and reveal that the competition between the two magnetic interactions is the decisive factor for the IC magnetic transition. Eventually, by analyzing the doping-controlled spin splitting of $d_{x^2-y^2}$ band and orbital-contributed exchange interactions, direct links between hole doping, magnetization, exchange constants, and magnetic order are established. This discovery of the IC spin state, new understanding of its electronic origin, and establishment of direct connection with the paring $d_{x^2-y^2}$ electrons radically change the current understanding of the magnetic properties in hole-doped $NdNiO_2$ and open new perspectives for the superconducting mechanism in nickelates superconductors.

1. Introduction

Infinite-layer nickelates $RNiO_2$ (R = rare-earth ion) have recently generated broad interest owing to the discovery of superconductivity.[1–41] This new class of hole-doped superconductors not only fuels theoretical and experimental research seeking new superconductors but also acts as a unique and valuable system for revealing the key ingredients responsible for the pairing mechanism of superconductivity. Magnetic interactions are commonly believed to play essential roles in the emergence of superconductivity,[42–44] so rationalizing the existence and origin of magnetism appears as a critical step in the understanding of the superconductivity mechanism.

Despite the importance of understanding the magnetic order, the magnetic ground state of infinite-layer nickelates remains unclear. In the undoped system, it is believed that cuprates are characterized by strongly 2D antiferromagnetic (AFM) interactions[45] while ferropnictides exhibit essentially 3D magnetism.[46] In nickelates, several works predict the magnetic ground state as 3D G-AFM or C-AFM, with notable interlayer magnetic coupling.[4–9] However, these studies give diverse pictures of the magnetic interactions. Recent resonant inelastic X-ray scattering (RIXS) experiment provides the necessary data for validating the computational approaches. It suggests instead a 2D magnetic coupling in $NdNiO_2$ similar to that of $CaCuO_2$ based on the unnoticeable dispersion along the specific (0.25, 0, 0.25)–(0.25, 0, 0.39) path,[23] which was not captured by previous calculations.

Y. Zhang
Key Laboratory of Mechanics on Disaster and Environment in Western China
Ministry of Education of China
Lanzhou University
Lanzhou, Gansu 730000, China
E-mail: zhangyajun@lzu.edu.cn

Y. Zhang
Department of Mechanics and Engineering Sciences
College of Civil Engineering and Mechanics
Lanzhou University
Lanzhou, Gansu 730000, China

The ORCID identification number(s) for the author(s) of this article can be found under https://doi.org/10.1002/adfm.202304187

DOI: 10.1002/adfm.202304187

X. He, P. Ghosez
Theoretical Materials Physics
Q-MAT
CESAM
Université de Liége
Liége B-4000, Belgium

J. Zhang, J. Wang
Department of Engineering Mechanics and Key Laboratory of Soft Machines and Smart Devices of Zhejiang Province
Zhejiang University
38 Zheda Road, Hangzhou 310027, China

J. Zhang, J. Wang
Zhejiang Laboratory
Hangzhou, Zhejiang 311100, China

A careful choice of the computational methods and parameters is thus not only essential for elucidating the magnetic mechanism in the undoped structure but also provides the basis for the prediction of the magnetic property in the doped structure.

For hole-doped superconductors, incommensurate (IC) spin order is one of the most intriguing and generic features of cuprates and iron superconductors and plays an important role in the superconducting phase diagram.[42–44] Interestingly, the superconducting phase diagram of infinite-layer nickelates is strikingly similar to that of cuprates.[12] Given the similar electronic configuration and magnetic excitations in their parent compounds, it is natural to wonder if there is similar IC magnetic order in hole-doped nickelate superconductors.

Herein, we provide compelling evidence of the appearance of IC spin state in hole-doped $NdNiO_2$ by employing the generalized Bloch theorem (GBT) and magnetic force theorem (MFT). We found that hole doping has profound impacts on the first-neighbor (J_1) and third-neighbor (J_3) in-plane exchange interactions and the two exchange interactions notably affect the incommensurability. Our Heisenberg model reveals that the amplitude of incommensurability is determined by J_1/J_3 ratio. The analysis of hole doping determined electronic structure and orbitals-contributed exchange constants highlight that the main roles of hole doping are to control the sign and J_1/J_3 ratio, which eventually determines the magnetic ground state and the incommensurability. Therefore, our work outlines a simple and unified mechanism for the commensurate-IC transition, with the first-neighbor and third-neighbor in-plane exchange interactions serving as the link between the hole doping and magnetic state.

2. Results and Discussion

2.1. Magnetic Ground State and Reliable Hubbard U

Various theoretical works based on first-principles calculations have already investigated the electronic and magnetic properties of $NdNiO_2$. However, different density functionals and Hubbard U values employed give quantitatively different predictions of the magnetic order, Fermi surface, and strength of magnetic interactions. This motivates a careful selection of functional and Hubbard U that can correctly match the experimental observations. Based on the selected functional, we will extend our understanding of the magnetic properties and their electronic origin. Moreover, this will provide the basis for reliable predictions of the electronic and magnetic properties in hole-doped systems.

A recent experiment has pointed out strong in-plane dispersion of magnetic excitations and unnoticeable dispersion along a q-path in the out-of-plane direction in $NdNiO_2$.[23] The comparison of measured magnetic dispersions with theoretical predictions offers a reliable basis to clarify the appropriate functional.

We first focus on the weak out-of-plane dispersion, which reveals negligible out-of-plane magnetic coupling and is in line with the fact that G-AFM and C-AFM states are close in energy. The schematic pictures of the different magnetic orders are plotted in Figure S1, Supporting Information. Figure S2a, Supporting Information displays the total energy difference between C-AFM and G-AFM states from the PBE + U method in their fully relaxed ground state *I4/mcm* phase with the existence of oxygen-square rotation (see Figures S3 and S4a,b, and the discussion, Supporting Information). It is found that there is a transition from the G-AFM to C-AFM state for PBE + U with U = 0.84 eV, indicating weak out-of-plane magnetic interactions. We further analyze the in-plane (J_1) and out-of-plane (J_5) first-neighbor exchange constants as a function of U values with their magnetic ground state phases. Figure S2b, Supporting Information, highlighting the out-of-plane exchange constant, shows a discontinuity for increasing U values, corresponding to a transition between two magnetic states consisting of i) a quasi-2D AFM state with mainly in-plane magnetic coupling, and ii) a weakly 3D C-AFM magnetic order with small while non-negligible out-of-plane ferromagnetic (FM) coupling. The intriguing discontinuity of the J value is due to the difference in the orbital occupation in the two states, which will be discussed later. Due to the negligible out-of-plane exchange constant in the G-AFM state of our simulations, it is reasonable to refer to that state as quasi-2D AFM in the following. An explicit comparison of exchange constants obtained from our PBE + U and strongly constrained and appropriately normed (SCAN) functional[48] calculations with previous computations and the experimental data is listed in Table S1, Supporting Information: it appears that our results are comparable, and even in closer agreement with experimental data[23] than previous predictions.[5,9,27,28]

To further confirm the reliable Hubbard U value and possible magnetic ground state, we have compared the experimental measurements and the predicted magnetic excitation spectrum obtained from a 2D-AFM state (**Figure 1**a) with U equal to 0.83 eV and from a 3D C-AFM state with a small out-of-plane FM coupling (Figure 1b) with U equal to 0.84 eV. Obviously, the magnetic dispersion curves obtained from both the 2D (Figure 1c) and weaky 3D (Figure 1d) models accurately reproduce the RIXS results,[23] including the absence of noticeable dispersion along the (0.25, 0, 25)–(0.25, 0, 0.39) path. However, our 3D model highlights pronounced dispersion along the Γ-Z direction not captured by the 2D model. The improved dispersion of M-Γ line in Figure 1d compared with experiments should be attributed to the smaller J_3 in the 3D C-AFM state (see Table S1, Supporting Information) since relative larger J_3 in the 2D-AFM state slightly overestimates the dispersion (see Figure S5, Supporting Information).

Interestingly, although the two possible states are very close in energy, they have strikingly different electronic structures. In the quasi-2D AFM state, the Fermi level is dominated by the Ni $d_{x^2-y^2}$ electrons (Figure 1e). In the weakly 3D C-AFM state, the itinerant Ni $d_{3z^2-r^2}$ orbitals intersect the Fermi level, while the Ni $d_{x^2-y^2}$ electrons are strongly localized below the Fermi level (Figure 1e). The orbital contributions of the exchange constants are listed in **Table 1**. We see clearly that the first-neighbor in-plane magnetic coupling (J_1) in both the quasi-2D AFM and weakly 3D C-AFM states mainly originates from the contribution of the localized Ni $d_{x^2-y^2}$ orbitals. Nevertheless, the presence of first-neighbor out-of-plane FM coupling (J_5) in the weakly 3D C-AFM state emerges from the interactions between the itinerant Ni $d_{3z^2-r^2}$ electrons. Consequently, a direct relationship between the Fermi surface and magnetic order is established: i) the localized $d_{x^2-y^2}$ electrons alone are responsible for the 2D magnetic dimensionality; ii) the itinerant Ni $d_{3z^2-r^2}$ and localized $d_{x^2-y^2}$ electrons account together for the 3D magnetic state in C-AFM $NdNiO_2$.

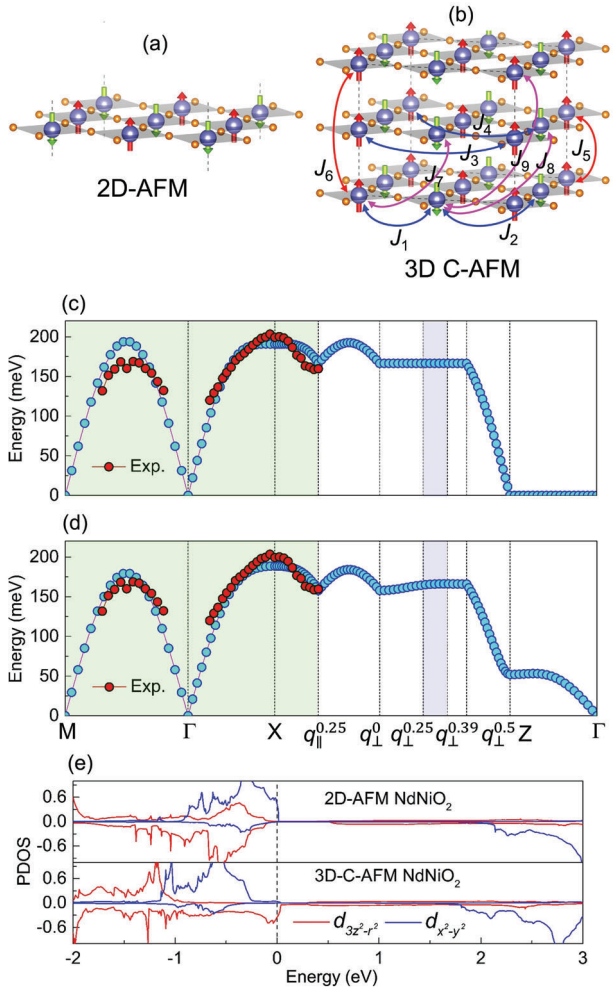

Figure 1. Magnetic dimensionality of $NdNiO_2$ and the electronic origin. Schematic representation of a) 2D-AFM and b) 3D C-AFM states with different neighboring exchange interactions. The simulated adiabatic spin-wave dispersions based on c) 2D-AFM model with Perdew–Burke–Ernzerhof (PBE)[47] + U[62] (U = 0.83 eV) and d) 3D C-AFM model with PBE + U (U = 0.84 eV) along different paths of the Brillouin zone of the tetragonal phase. The experimental results[23] in red circles are also shown for comparison. Here, M = (0.5, 0.5, 0), Γ = (0, 0, 0), X = (0.5, 0, 0), $q_{\parallel}^{0.25}$ = (0.5, 0.25, 0), $q_{\perp}^{0}$ = (0.25, 0, 0), $q_{\perp}^{0.25}$ = (0.25, 0, 0.25), $q_{\perp}^{0.39}$ = (0.25, 0, 0.39), $q_{\perp}^{0.5}$ = (0.25, 0, 0.5), and Z = (0, 0, 0.5). A segment of the path $q_{\perp}^{0.25}$-$q_{\perp}^{0.39}$ with a background in blue is taken in Ref. [23] to show the flatness of the dispersion along the out-of-plane direction. e) Projected density of states (PDOS) of Ni atoms for quasi-2D-AFM and 3D C-AFM $NdNiO_2$. The Fermi level denoted by the dash line is set to zero energy.

Overall, our results establish the ability of the PBE + U method to correctly capture the experimentally measured magnetic dispersion and fitted exchange constants of $NdNiO_2$. Doing so, they unveil the existence of two competing magnetic states, which both show good consistency with current experiments, so that the determination of the exact magnetic dimensionality and ground state calls for further experimental measurements of magnetic dispersion along other out-of-plane directions. Despite this remaining ambiguity for the undoped system, we will demonstrate in the following that our central finding of IC magnetic order in a hole-doped system is an intrinsic feature, which is mainly determined by the competing in-plane exchange interactions. Whether the undoped system has a 2D or 3D magnetic ground state does not affect this result, which appears therefore extremely robust.

2.2. IC Magnetic Order in Hole-Doped $NdNiO_2$

Having obtained an appropriate description of the magnetic interactions in the undoped $NdNiO_2$, we now explore further the possible occurrence of an IC spin state in hole-doped $NdNiO_2$ by comparing the total energies E(q) of the spin spiral states with different wave vector q using the GBT.[49] As the accurate spin spiral calculations need very condensed k-points and the calculations in the *I4/mcm* phase is very costly, we use the unit-cell of high-symmetry *P4/mmm* phase (all the atoms occupying the high-symmetry positions as shown in Figure S4c,d, Supporting Information) to predict a spin spiral state for simplicity. Nevertheless, we have clearly demonstrated in Figure S6, Supporting Information that the amplitude of incommensurability δ would not be strongly affected by the structure used and the initial spin state (2D-AFM or 3D C-AFM) in the parent $NdNiO_2$. **Figure 2**a presents the energy difference ΔE between the spin spiral states and 2D-AFM state at 0.18 hole doping, in the middle of the superconducting regime ($0.125 \leq x \leq 0.25$).[12] It is obvious from Figure 2a that the state with $q_x = q_y = 0.26$ is the most energetically favorable phase, which is a definitive signature of IC magnetic order. Using the same method, the incommensurability δ ($\delta = 0.5-q$) from lightly doped to overdoped states is summarized in Figure 2b. Interestingly, the features are analogous to $La_{2-x}Sr_xCuO_4$[44] which δ varies with Sr doping: i) the IC state occurs before the transition to the superconducting phase; ii) the incommensurability δ increases almost linearly with doping when it starts to across the superconducting phase boundary. Overall, the similarity of the IC magnetic state in $NdNiO_2$ and cuprate superconductors over a wide range of doping indicates that the IC spin state is robust and a general feature of hole-doped superconductors, which could be naturally extended to infinite-layer nickelates.

While the IC spin order in nickelate superconductors is directly confirmed by the GBT, this approach alone is inadequate to identify the microscopic origin of magnetic

Table 1. First-neighbor exchange constants of $NdNiO_2$ in the unit of meV. The in-plane (J_1) and out-of-plane (J_5) first-neighbor exchange constants and their orbital contributions in the 2D-AFM states (PBE + U (U = 0.83 eV)) and 3D C-AFM states (PBE + U (U = 0.84 eV)).

J values	J_1 (U = 0.83 eV)	J_1 (U = 0.84 eV)	J_5 (U = 0.84 eV)
Total	76.99	78.84	−3.34
$d_{x^2-y^2}$-$d_{x^2-y^2}$	65.45	71.92	−0.21
$d_{x^2-y^2}$-d_{xy}	10.76	6.16	−0.15
$d_{3z^2-r^2}$-$d_{3z^2-r^2}$	0.19	0.20	−3.43
$d_{x^2-y^2}$-$d_{3z^2-r^2}$	−0.02	0.30	0.00
d_{xy}-d_{xy}	0.69	0.28	0.05
d_{xz}-d_{xz}	0.08	0.06	0.20
d_{yz}-d_{yz}	−0.16	−0.08	0.20

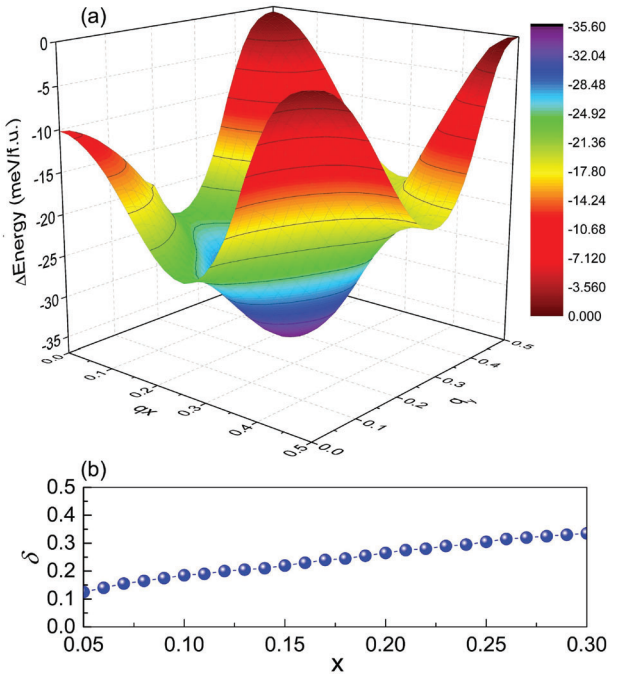

Figure 2. Verification of IC magnetic ground state in hole-doped $NdNiO_2$. a) The energy difference ΔE between different spin spiral states and 2D-AFM state for $Sr_{0.18}Nd_{0.82}NiO_2$. b) Doping concentration dependent incommensurability δ.

incommensurability. Here, an alternative and easier method based on the calculated exchange constants with MFT[50] from the FM state is employed to determine the incommensurability δ. This method is exact when the spin state is in the first-principles reference state, and becomes an approximation otherwise. A good approximation requires the electronic structure to be similar to the reference state. As δ is larger than 0.25 for the range of doping $0.16 \leq x \leq 0.3$, the in-plane first-neighbor exchange interaction should be close to the FM alignment, therefore, the A-AFM state can be a good approximation of the IC state. Indeed, the IC spin state for $0.05 \leq x < 0.16$ cannot be predicted by the MFT from the J values computed with the G-AFM electronic structure in which the $d_{x^2-y^2}$ bandwidth is smaller than the A-AFM state. Thus, we use this method to analyze the case of $0.16 \leq x \leq 0.3$. In **Figure 3**a, we display δ in terms of the doping concentration. Clearly, the monotonic increase and δ values agree reasonably well with the results from spin spiral calculations using GBT, attesting that the MFT gives a good approximation. The consistent results from two entirely different approaches not only provide convincing evidence for the IC nature of magnetic order but also demonstrate that our predictions are not the artifact of a specific method.

2.3. Origin of IC Magnetic Order

To reveal the microscopic origin of the IC spin state, we first compare the change of exchange constants as a function of doping. From Figure S7, Supporting Information, we notice that the in-plane magnetic interactions are mostly dominated by the first-neighbor, second-neighbor, third-neighbor, and fourth-neighbor exchange interactions, which are schematically shown in Figure 1b. Figure 3b displays the variation of four exchange constants as a function of hole doping. It is clear that J_1 evolves much faster than the other interactions and the strength shows an almost linear decrease (increase) in the AFM (FM) region. Moreover, the first-neighbor magnetic coupling undergoes an AFM-FM transition at the hole concentration of $x = 0.15$, which is accompanied by the FM-AFM transition of the second-neighbor and third-neighbor magnetic couplings. Strikingly, the strength of J_3 becomes comparable to that of J_1 at a relatively high doping concentration. The J values are approximated by perturbing the two different collinear spin states with the lowest energy, which are G-AFM and A-AFM below and above $x = 0.15$, respectively. This leads to a sign change of the J values at $x = 0.15$. The bandwidth of the $d_{x^2-y^2}$ orbital is much larger in the A-AFM structure than in the G-AFM structure as shown in the next section, which

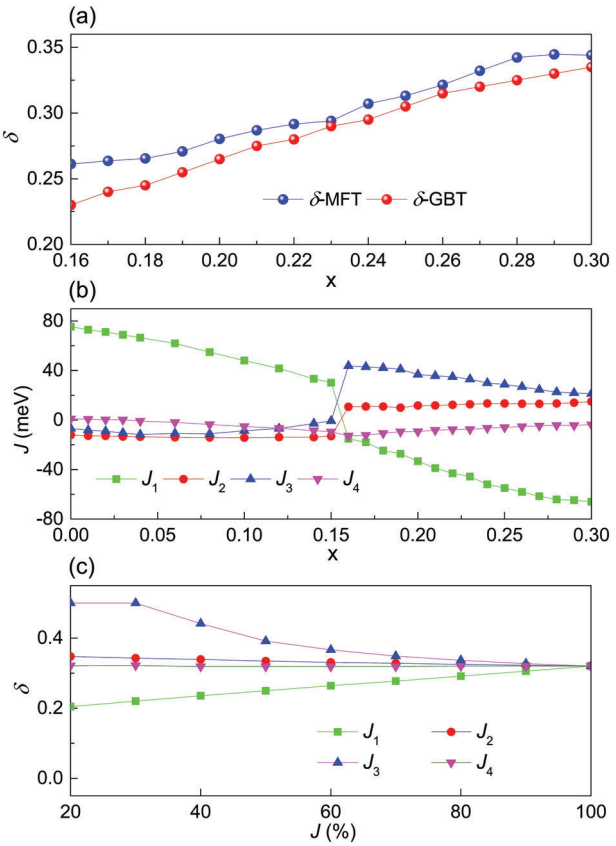

Figure 3. The microscopic origin of the IC magnetic state. a) The comparison of incommensurability δ from the MFT and GBT. b) The variation of dominant exchange constants as a function of doping level x. The J values are computed from the lowest-energy collinear spin calculations, specifically, the G-AFM ($x \leq 0.15$) and the A-AFM states ($x \geq 0.16$). Positive values correspond to AFM coupling. c) The evolution of incommensurability δ when changing one specific J value in $Sr_{0.25}Nd_{0.75}NiO_2$. In the calculations, we vary one of the four dominant J values while fixing the other three to the values of $Sr_{0.25}Nd_{0.75}NiO_2$. Here, green, red, blue, and magenta curves represent the change of δ when varying J_1, J_2, J_3, and J_4, respectively. 0% denotes the specific J value in $NdNiO_2$, and 100% represents the corresponding J value in $Sr_{0.25}Nd_{0.75}NiO_2$.

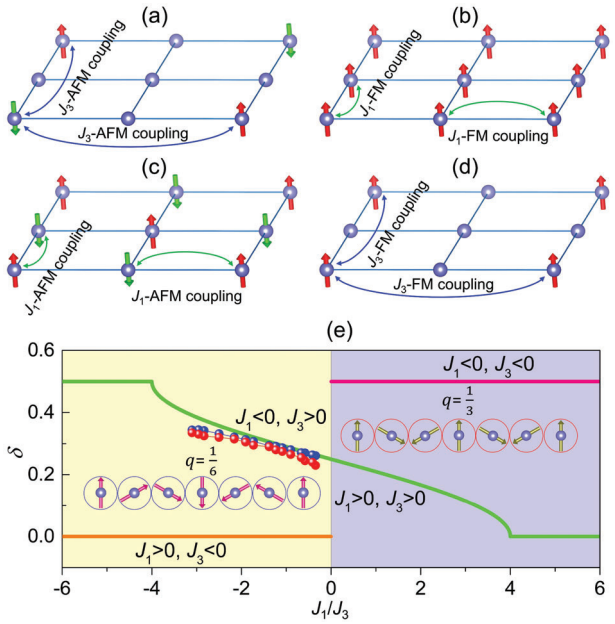

Figure 4. Schematic representation of the alignments of magnetic moments of Ni ions controlled by different magnetic interactions. The alignments of magnetic moments induced by a) third-neighbor AFM coupling, b) first-neighbor FM coupling, c) first-neighbor AFM coupling, and d) third-neighbor FM coupling. e) The analytical solution of δ_* from the J_1-J_3 model. The MFT (blue ball) and GBT (red ball) results from Figure 3a with the J_1/J_3 ratio from MFT are also plotted together for comparison. The sketches of spin waves (q = 1/6 and 1/3) highlight the region of FM (resp. AFM) in-plane first-neighbor magnetic interaction.

enhances the hole-doping in the $d_{x^2-y^2}$ band, and in turn, stabilizes the first-neighbor FM interaction.

Next, we elucidate how the IC spin state and δ connect to the variation of these magnetic interactions. Taking $Sr_{0.25}Nd_{0.75}NiO_2$ as an example, Figure 3c shows the evolution of incommensurability δ when we gradually change one of the four dominant exchange interactions in $Sr_{0.25}Nd_{0.75}NiO_2$. One can see that δ depends crucially on the first-neighbor and third-neighbor magnetic interactions while is only slightly affected by the second-neighbor and fourth-neighbor magnetic interactions. In detail, we found that δ increases almost linearly when the first-neighbor magnetic interaction gradually changes from strong AFM interaction to strong FM interaction. Intriguingly, δ is strongly reduced with the weakening of third-neighbor AFM magnetic interaction, and the IC state is completely suppressed when the third-neighbor magnetic interaction becomes FM, indicating the decisive role of the third-neighbor AFM magnetic interaction for the emergence of IC state.

The impact of first- and third-neighbor exchange constants on the magnetic order can be qualitatively explained as follows: i) For AFM J_3 as shown in **Figure 4**a, we see that it favors an AFM alignment of the in-plane third-neighbor magnetic moments. In contrast, eitherFM J_1 that favors the commensurate FM state (see Figure 4b) or AFM J_1 that favors the commensurate AFM state (see Figure 4c) would lead to an FM alignment of the in-plane third-neighbor magnetic moments. Therefore, the actual alignment of the in-plane third-neighbor magnetic moments is determined by the competing effects of J_1 and J_3, thus, the balance of the competition is decisive for the incommensurability; ii) For FM J_3 (see Figure 4d), J_1 and J_3 cooperate and both favor FM alignment of the in-plane third-neighbor magnetic moments, as a result, the magnetic ground state becomes commensurate when J_3 turns FM.

To further clarify the role of the first-neighbor and third-neighbor magnetic interactions in the origin of the IC state, we analyze a simplified J_1-J_3 Heisenberg model by eliminating the other exchange interactions:

$$E = -\sum_{R\in 1N} J_1 S(0)\, S(R) - \sum_{R\in 3N} J_3 S(0)\, S(R) \tag{1}$$

Where $R \in 1N$ and $R \in 3N$ mean the first-neighbor and third-neighbor, respectively. For a spin spiral state, the wave vector $\vec{q}_*$ can be written as $S_{\vec{q}_*}(R) = Se^{i\vec{q}_*\cdot\vec{R}}$, we can evaluate the energy as a function of $\vec{q}_*$ and find its minimum.

With a FM J_3 ($J_3 < 0$), the magnetic structure is commensurate and the order depends on J_1. The wave vector is $q_* = 0$ when J_1 is FM, and is $q_* = 1/2$ when J_1 is AFM. With an AFM J_3 ($J_3 > 0$), the wave vector q_* depends on the ratio of J_1/J_3:

$$q_* = \begin{cases} 0, \text{if } -\frac{J_1}{4J_3} > 1 \\ \frac{1}{2}, \text{if } -\frac{J_1}{4J_3} < -1 \\ \frac{1}{2\pi}\arccos\left(-\frac{J_1}{4J_3}\right), \text{if } -1 < -\frac{J_1}{4J_3} < 1 \end{cases} \tag{2}$$

here, q_* has the unit of $2\pi/a$. The dependence of δ_* on the J_1/J_3 ratio is shown in Figure 4e, the results from GBT and MFT shown in Figure 3a are also plotted for comparison. The numerical solutions agree well with the results obtained from both the GBT and MFT (with all the exchange constants) methods, indicating the effectiveness of the J_1-J_3 model and critical role of J_1/J_3 ratio for incommensurability δ.

2.4. Doping-Spin Splitting-Exchange Interactions-Magnetic Order Relationship

Nowadays, it is proposed that the IC spiral state coexists and couples with superconductivity. However, the microscopic origin of this specific phase remains controversial. Fermi surface topology,[51] dipolar distortion,[52] next-nearest neighbor hopping,[53] stripe-domain,[54] and interaction between holes[55] have been proposed to be responsible for the IC spiral state. In the above discussions, we propose a different perspective by establishing a direct relationship between the electronic structure, the exchange constant, and the IC state. Then, the key question is how this mechanism is connected to the $d_{x^2-y^2}$ band which is the origin of the pairing interaction.[56]

To answer this question and gain further insight into the relationship between the magnetic interaction and the electronic states, we first focus on the effect of doping on the electronic structure. The hole-doping dependence of PDOS of Ni $d_{x^2-y^2}$ band in lightly doped states and moderately doped states are shown in **Figure 5**a,b. Consistently with recent experiments,[2] we found that Sr doping has a strong effect on the Ni d orbitals. From small to large doping concentrations (i.e., increasing x),

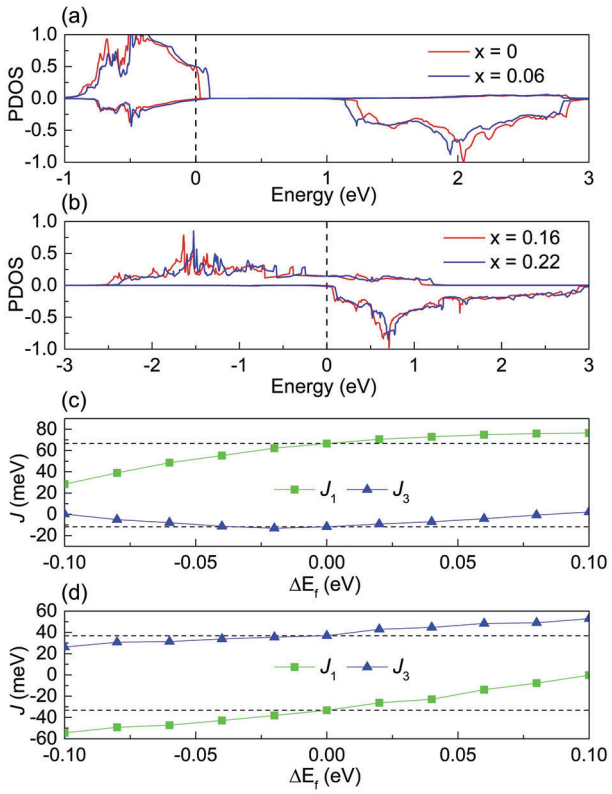

Figure 5. The hole doping-magnetization-magnetic interactions relationship. The PDOS for $d_{x^2-y^2}$ band of Ni atom in $Sr_xNd_{1-x}NiO_2$ with a) G-AFM state for undoped and lightly doped states and b) A-AFM state for moderately doped states. The effect of the shift of Fermi energy (E_f) on the J_1 and J_3 for c) $Sr_{0.04}Nd_{0.96}NiO_2$ and d) $Sr_{0.2}Nd_{0.8}NiO_2$. In (c) and (d), the dash lines are the values without Fermi energy shifting.

one can observe that the spin polarization gradually decreases, and the Fermi level shifts down continuously, in line with previous works.[13,35]

In order to elucidate how the magnetic interactions are influenced by the reduction of spin polarization, we employed a rigid band approximation to decouple the effect due to the rigid Fermi shift from the variation of the band structure, which helps to understand how doping affects the exchange constants. In detail, we artificially shift the Fermi level of $Sr_{0.04}Nd_{0.96}NiO_2$ (Figure 5c) and $Sr_{0.2}Nd_{0.8}NiO_2$ (Figure 5d) and calculate the exchange constants at each state. Strikingly, both J_1 and J_3 are dominated by the magnetic interactions from the $d_{x^2-y^2}$ bands, as evidenced in Table S2, Supporting Information. The evolutions of J_1 and J_3 are presented in Figure 5c,d. As the Fermi level shifts down, for $Sr_{0.04}Nd_{0.96}NiO_2$ with first-neighbor AFM interactions, J_1 is more sensitive to the reduction of spin polarization and decreases more quickly than the increase of FM J_3. According to the phase diagram in Figure 4e, the decrease of the J_1/J_3 ratio directly triggers the commensurate-IC transition and causes the increase of incommensurability δ. In terms of $Sr_{0.2}Nd_{0.8}NiO_2$ with first-neighbor FM interactions, J_1 increases much faster than the weakening of AFM J_3 as the Fermi level shifts down. This results in the increase of the J_1/J_3 ratio and consequently increases the incommensurability δ based on the phase diagram shown in Figure 4e. Obviously, we can see that the results from rigid band shift (see Figure 5c,d) well reproduce the main trend of the change of the exchange parameters as a function of hole doping shown in Figure 3b. The rigid band approximation unambiguously confirms that the weakening of the magnetization of the $d_{x^2-y^2}$ band contributes to the large variations of J_1, J_3, and J_1/J_3 ratio. The change of J_1/J_3 ratio then controls the IC spin state and variation of incommensurability δ. Therefore, we provide a clear electronic origin of the change of J_1 and J_3 and establish a clear connection between the hole doping, magnetization of $d_{x^2-y^2}$ band, the variation of exchange constant, and the IC spin state.

It should be noticed that in our calculations with GBT and MFT, a homogeneous spin/charge density on the Ni sites is assumed. In high-T_c superconductors, other states like spin/charge density wave[36–38,54,57] and nematic states[58] have been proposed, and are often considered to be related to the superconductivity. Our simulations with reasonable Hubbard U and static correction cannot show such evidence. Quite a large U value (U = 5 eV) is possible to stabilize the charge density state,[33] while such a high U value significantly overestimates the Ni-O-Ni rotation angle, strongly underestimates the first-neighbor exchange constant (see Figure S8, Supporting Information) and provides inconsistent excitation spectra compared with experiments (see Figure S9, Supporting Information). In contrast, despite two competing and possible magnetic ground states having been revealed in the undoped state, the breaking of the commensurate magnetic order from our prediction seems to be intrinsic and robust and is not affected by the selected Hubbard U, the magnetic ground state in undoped $NdNiO_2$ (C-AFM or 2D-AFM), mismatch strain ($NdNiO_2$ thin film grown on $SrTiO_3$ substrate), and the rotation distortion (see Figure S6, Supporting Information).

3. Conclusion

We have presented a systematic theoretical investigation of the magnetic properties in infinite-layer nickelates. The experimentally measured magnetic excitation spectrum in undoped $NdNiO_2$ has been first reproduced by first-principles and spin-wave theory calculations. This has validated the exchange-correlation functional and the Hubbard U while also revealing the existence of two competitive magnetic ground states. Based on the method, we have then revealed that hole hoping strongly affects the spin splitting of the Ni $d_{x^2-y^2}$ bands, magnetic coupling strength, and magnetic order, which naturally triggers a transition to the IC spin order. This provides a natural way to connect superconducting nickelates with hole-doped iron-and copper-based superconductors and helps narrow down the key factors in determining the superconductivity of high-T_c superconductors. The results are robust and independent of the original ground state of the undoped system. A consistent model connecting the magnetization, exchange interaction, and magnetic order has been established. The hole-doping tuned nature of first-neighbor and third-neighbor magnetic interactions (AFM or FM) and their ratio are revealed to be decisive factors for the magnetic ground state. Our results provide a new intriguing insight into the microscopic origin of the IC spin state and might be instrumental for rationalizing the mechanism of superconductivity.

4. Experimental Section

First-Principles Calculations: The first-principles calculations were performed using the projector augmented wave (PAW) method implemented in the VASP code.[59,60] SCAN functional[48] was known to overestimate the magnetization and magnetic energies of metals,[61] for a better description of the magnetic property, PBE[47] + U[62] method was employed. Hubbard U of 0.83 eV was employed in most of the calculations if it is not mentioned. Here, 4*f* electrons were not considered since they are far away from the Fermi energy.[63] An energy cutoff of 700 eV was used, and the energy and force convergence criterions were set to be 10^{-7} eV and 10^{-3} eV Å^{-1} for the structural relaxation. The k-point meshes[64] were set to be 9 × 9 × 7 and 15 × 15 × 18 for the *I4/mcm* phase and *P4/mmm* unit cell. The doping of Sr was simulated by virtual crystal approximation (VCA). The energies of the spin spiral states were computed with the GBT. The phonon dispersion curves were calculated by the finite displacement method as implemented in the PHONOPY code.[65]

Exchange Constant and Magnetic Excitations Calculations: The exchange constants and the orbital contributions were obtained by the MFT[50] as implemented in the TB2J code[66] using maximally localized Wannier functions.[67,68] Here, Nd d_{xy} and $d_{3z^2-r^2}$ orbitals, Ni d_{xy}, d_{yz}, d_{zx}, $d_{x^2-y^2}$, and $d_{3z^2-r^2}$ orbitals and O p_x, p_y, and p_z orbitals were used for the construction of the Wannier functions. In the simulations, G-AFM state was used for the undoped and lightly doped states, and the A-AFM state was used for the moderately doped states, which are the collinear spin ground states.

The Heisenberg Hamiltonian can be expressed as follows:

$$H = \sum_{\langle i,j \rangle} J_{ij} S_i S_j \tag{3}$$

Here, J_{ij} is the exchange constant at any order and $S = 1/2$ spin.

The expression for the exchange parameter from the MFT can be written as:[50,66,69]

$$J_{ij} = \frac{2}{\pi} \int_{-\infty}^{E_F} \mathrm{Im}\mathrm{Tr}\Delta_i G_{ij}^{\uparrow} \Delta_j G_{ji}^{\downarrow} d\epsilon \tag{4}$$

in which, H is the tight-binding Hamiltonian, G is the Green's function from the Hamiltonian, $G(\epsilon) = (\epsilon I - H)^{-1}$, $\Delta_i = H_i^{\uparrow} - H_i^{\downarrow}$ which is the difference between the spin-up and spin-down part of the sub-matrix of H on one atom *i*. (Note that there is a prefactor difference of -8 in the formulations in Ref. [50] and Ref. [66] due to the different conventions of the Heisenberg model adopted.

The exchange parameter can be decomposed as the sum of the contributions from orbital pairs in two atoms:[50]

$$J_{im,jm'} = \frac{2}{\pi} \mathrm{Im} \int_{-\infty}^{E_F} \Delta_{im} G_{im,jm'}^{\uparrow} \Delta_{jm'} G_{jm',im}^{\downarrow} d\epsilon \tag{5}$$

m and *m'* are the orbital indices.

As the exchange parameters are computed by integrating over energy up to the Fermi energy ($\int_{-\infty}^{E_F} |\cdot$ as in Equation (4) and Equation (5)), the contribution from the states at the Fermi energy can easily be found by varying the E_F. This provides an easy way to study the effect of electron occupation on the exchange interactions. The spin-wave spectra are calculated by the SpinW program[70] based on the obtained exchange constants.

Supporting Information

Supporting Information is available from the Wiley Online Library or from the author.

Acknowledgements

Y.Z. and X.H. contributed equally to this work. The authors thank the computational support from the Center for Computational Science and Engineering of Lanzhou University. Y.Z. acknowledges support by the Initial Scientific Research Fund of Lanzhou University for Young Researcher Fellow (Grant No. 561120206) and the National Natural Science Foundation of China (Grant No. 12102157). J.W. acknowledges the financial support from National Program on Key Basic Research Project (Grant No. 2022YFB3807601). Ph.G. and X.H. acknowledge financial support from F.R.S.-FNRS Belgium through the PDR project PROMOSPAN (Grant No. T.0107.20).

Conflict of Interest

The authors declare no conflict of interest.

Data Availability Statement

The data that support the findings of this study are available from the corresponding author upon reasonable request.

Keywords

competing magnetic interactions, incommensurate spin state, infinite-layer nickelates, nonlinear Heisenberg model

Received: April 16, 2023
Revised: June 13, 2023
Published online:

[1] D. Li, K. Lee, B. Y. Wang, M. Osada, S. Crossley, H. R. Lee, Y. Cui, Y. Hikita, H. Y. Hwang, *Nature* **2019**, *572*, 624.
[2] M. Osada, B. Y. Wang, B. H. Goodge, K. Lee, H. Yoon, K. Sakuma, D. Li, M. Miura, L. F. Kourkoutis, H. Y. Hwang, *Nano Lett.* **2020**, *20*, 5735.
[3] M. Hepting, D. Li, C. Jia, H. Lu, E. Paris, Y. Tseng, X. Feng, M. Osada, E. Been, Y. Hikita, Y.-D. Chuang, Z. Hussain, K. J. Zhou, A. Nag, M. Garcia-Fernandez, M. Rossi, H. Y. Huang, D. J. Huang, Z. X. Shen, T. Schmitt, H. Y. Hwang, B. Moritz, J. Zaanen, T. P. Devereaux, W. S. Lee, *Nat. Mater.* **2020**, *19*, 381.
[4] J. Kapeghian, A. S. Botana, *Phys. Rev. B* **2020**, *102*, 205130.
[5] Z. Liu, Z. Ren, W. Zhu, Z. Wang, J. Yang, *npj Quantum Mater.* **2020**, *5*, 31.
[6] I. Leonov, S. Skornyakov, S. Savrasov, *Phys. Rev. B* **2020**, *101*, 241108.
[7] S. Ryee, H. Yoon, T. J. Kim, M. Y. Jeong, M. J. Han, *Phys. Rev. B* **2020**, *101*, 064513.
[8] A. Botana, M. Norman, *Phys. Rev. X* **2020**, *10*, 011024.
[9] R. Zhang, C. Lane, B. Singh, J. Nokelainen, B. Barbiellini, R. S. Markiewicz, A. Bansil, J. Sun, *Commun. Phys.* **2021**, *4*, 1.
[10] M.-Y. Choi, W. E. Pickett, K.-W. Lee, *Phys. Rev. Res.* **2020**, *2*, 033445.
[11] V. M. Katukuri, N. A. Bogdanov, O. Weser, J. Van den Brink, A. Alavi, *Phys. Rev. B* **2020**, *102*, 241112.
[12] D. Li, B. Y. Wang, K. Lee, S. P. Harvey, M. Osada, B. H. Goodge, L. F. Kourkoutis, H. Y. Hwang, *Phys. Rev. Lett.* **2020**, *125*, 027001.
[13] J. Krishna, H. LaBollita, A. O. Fumega, V. Pardo, A. S. Botana, *Phys. Rev. B* **2020**, *102*, 224506.
[14] S. Zeng, C. S. Tang, X. Yin, C. Li, M. Li, Z. Huang, J. Hu, W. Liu, G. J. Omar, H. Jani, Z. S. Lim, K. Han, D. Wan, P. Yang, S. J. Pennycook, A. T. S. Wee, A. Ariando, *Phys. Rev. Lett.* **2020**, *125*, 147003.

[15] F. Lechermann, *Phys. Rev. X* **2020**, *10*, 041002.
[16] F. Lechermann, *Phys. Rev. B* **2020**, *101*, 081110.
[17] P. Adhikary, S. Bandyopadhyay, T. Das, I. Dasgupta, T. Saha-Dasgupta, *Phys. Rev. B* **2020**, *102*, 100501.
[18] J. Karp, A. S. Botana, M. R. Norman, H. Park, M. Zingl, A. Millis, *Phys. Rev. X* **2020**, *10*, 021061.
[19] M.-Y. Choi, K.-W. Lee, W. E. Pickett, *Phys. Rev. B* **2020**, *101*, 020503.
[20] F. Petocchi, V. Christiansson, F. Nilsson, F. Aryasetiawan, P. Werner, *Phys. Rev. X* **2020**, *10*, 041047.
[21] M. Jiang, M. Berciu, G. A. Sawatzky, *Phys. Rev. Lett.* **2020**, *124*, 207004.
[22] Z. Wang, G.-M. Zhang, Y.-f. Yang, F.-C. Zhang, *Phys. Rev. B* **2020**, *102*, 220501.
[23] H. Lu, M. Rossi, A. Nag, M. Osada, D. F. Li, K. Lee, B. Y. Wang, M. Garcia-Fernandez, S. Agrestini, Z. X. Shen, E. M. Been, B. Moritz, T. P. Devereaux, J. Zaanen, H. Y. Hwang, K.-J. Zhou, W. S. Lee, *Science* **2021**, *373*, 213.
[24] B. Y. Wang, D. Li, B. H. Goodge, K. Lee, M. Osada, S. P. Harvey, L. F. Kourkoutis, M. R. Beasley, H. Y. Hwang, *Nat. Phys.* **2021**, *17*, 473.
[25] Y. Xiang, Q. Li, Y. Li, H. Yang, Y. Nie, H.-H. Wen, *Chin. Phys. Lett.* **2021**, *38*, 047401.
[26] F. Lechermann, *Phys. Rev. Mater.* **2021**, *5*, 044803.
[27] E. Been, W.-S. Lee, H. Y. Hwang, Y. Cui, J. Zaanen, T. Devereaux, B. Moritz, C. Jia, *Phys. Rev. X* **2021**, *11*, 011050.
[28] X. Wan, V. Ivanov, G. Resta, I. Leonov, S. Y. Savrasov, *Phys. Rev. B* **2021**, *103*, 075123.
[29] Y. Nomura, M. Hirayama, T. Tadano, Y. Yoshimoto, K. Nakamura, R. Arita, *Phys. Rev. B* **2019**, *100*, 205138.
[30] F. Bernardini, A. Bosin, A. Cano, *Phys. Rev. Mater.* **2022**, *6*, 044807.
[31] M. Rossi, H. Lu, A. Nag, D. Li, M. Osada, K. Lee, B. Y. Wang, S. Agrestini, M. Garcia-Fernandez, J. Kas, Y.-D. Chuang, Z. X. Shen, H. Y. Hwang, B. Moritz, K.-J. Zhou, T. P. Devereaux, W. S. Lee, *Phys. Rev. B* **2021**, *104*, L220505.
[32] J. Fowlie, M. Hadjimichael, M. M. Martins, D. Li, M. Osada, B. Y. Wang, K. Lee, Y. Lee, Z. Salman, T. Prokscha, J.-M. Triscone, H. Y. Hwang, A. Suter, *Nat. Phys.* **2022**, *18*, 1043.
[33] H. Chen, Y.-f. Yang, G.-M. Zhang, arXiv preprint arXiv:2204.12208 2022.
[34] A. Kreisel, B. M. Andersen, A. T. Romer, I. M. Eremin, F. Lechermann, *Phys. Rev. Lett.* **2022**, *129*, 077002.
[35] D. Chen, P. Jiang, L. Si, Y. Lu, Z. Zhong, *Phys. Rev. B* **2022**, *106*, 045105.
[36] C. C. Tam, J. Choi, X. Ding, S. Agrestini, A. Nag, M. Wu, B. Huang, H. Luo, P. Gao, M. Garcia-Fernández, L. Qiao, K.-J. Zhou, *Nat. Mater.* **2022**, *21*, 1116.
[37] G. Krieger, L. Martinelli, S. Zeng, L. Chow, K. Kummer, R. Arpaia, M. M. Sala, N. Brookes, A. Ariando, N. Viart, et al., *Phys. Rev. Lett.* **2022**, *129*, 027002.
[38] M. Rossi, M. Osada, J. Choi, S. Agrestini, D. Jost, Y. Lee, H. Lu, B. Y. Wang, K. Lee, A. Nag, Y.-D. Chuang, C.-T. Kuo, S.-J. Lee, B. Moritz, T. P. Devereaux, Z.-X. Shen, J.-S. Lee, K.-J. Zhou, H. Y. Hwang, W.-S. Lee, *Nat. Phys.* **2022**, *18*, 869.
[39] V. Christiansson, F. Petocchi, P. Werner, *Phys. Rev. B* **2023**, *107*, 045144.
[40] X. Liao, M. R. Norman, H. Park, *Phys. Rev. B* **2023**, *107*, 165153.
[41] X. Ding, C. C. Tam, X. Sui, Y. Zhao, M. Xu, J. Choi, H. Leng, J. Zhang, M. Wu, H. Xiao, X. Zu, M. Garcia-Fernandez, S. Agrestini, X. Wu, Q. Wang, P. Gao, S. Li, B. Huang, K.-J. Zhou, L. Qiao, *Nature* **2023**, *615*, 50.
[42] T. Moriya, K. Ueda, *Adv. Phys.* **2000**, *49*, 555.
[43] M. Kastner, R. Birgeneau, G. Shirane, Y. Endoh, *Rev. Mod. Phys.* **1998**, *70*, 897.
[44] R. J. Birgeneau, C. Stock, J. M. Tranquada, K. Yamada, *J. Phys. Soc. Japan* **2006**, *75*, 111003.
[45] Y. Endoh, K. Yamada, R. Birgeneau, D. Gabbe, H. Jenssen, M. Kastner, C. Peters, P. Picone, T. Thurston, J. Tranquada, G. Shirane, Y. Hidaka, M. Oda, Y. Hidaka, M. Oda, Y. Enomoto, M. Suzuki, T. Murakami, *Phys. Rev. B* **1988**, *37*, 7443.
[46] J. Zhao, D. Adroja, D.-X. Yao, R. Bewley, S. Li, X. Wang, G. Wu, X. Chen, J. Hu, P. Dai, *Nat. Phys.* **2009**, *5*, 555.
[47] J. P. Perdew, K. Burke, M. Ernzerhof, *Phys. Rev. Lett.* **1996**, *77*, 3865.
[48] J. Sun, A. Ruzsinszky, J. P. Perdew, *Phys. Rev. Lett.* **2015**, *115*, 036402.
[49] L. Sandratskii, *Adv. Phys.* **1998**, *47*, 91.
[50] A. I. Liechtenstein, M. Katsnelson, V. Antropov, V. Gubanov, *J. Magn. Magn. Mater.* **1987**, *67*, 65.
[51] Q. Si, Y. Zha, K. Levin, J. Lu, *Phys. Rev. B* **1993**, *47*, 9055.
[52] B. I. Shraiman, E. D. Siggia, *Phys. Rev. Lett.* **1989**, *62*, 1564.
[53] O. P. Sushkov, V. N. Kotov, *Phys. Rev. B* **2004**, *70*, 024503.
[54] J. Tranquada, B. Sternlieb, J. Axe, Y. Nakamura, S.-i. Uchida, *Nature* **1995**, *375*, 561.
[55] A. V. Chubukov, K. A. Musaelian, *Phys. Rev. B* **1995**, *51*, 12605.
[56] D. J. Scalapino, *Phys. Rep.* **1995**, *250*, 329.
[57] V. J. Emery, S. Kivelson, *Physica C Supercond.* **1993**, *209*, 597.
[58] M. Vojta, *Adv. Phys.* **2009**, *58*, 699.
[59] G. Kresse, J. Hafner, *Phys. Rev. B* **1993**, *47*, 558.
[60] P. E. Blöchl, *Phys. Rev. B* **1994**, *50*, 17953.
[61] Y. Fu, D. J. Singh, *Phys. Rev. Lett.* **2018**, *121*, 207201.
[62] S. Dudarev, G. Botton, S. Savrasov, C. Humphreys, A. Sutton, *Phys. Rev. B* **1998**, *57*, 1505.
[63] G.-M. Zhang, Y.-f. Yang, F.-C. Zhang, *Phys. Rev. B* **2020**, *101*, 020501.
[64] H. J. Monkhorst, J. D. Pack, *Phys. Rev. B* **1976**, *13*, 5188.
[65] A. Togo, F. Oba, I. Tanaka, *Phys. Rev. B* **2008**, *78*, 134106.
[66] X. He, N. Helbig, M. J. Verstraete, E. Bousquet, *Comput. Phys. Commun.* **2021**, *264*, 107938.
[67] N. Marzari, A. A. Mostofi, J. R. Yates, I. Souza, D. Vanderbilt, *Rev. Mod. Phys.* **2012**, *84*, 1419.
[68] A. A. Mostofi, J. R. Yates, G. Pizzi, Y.-S. Lee, I. Souza, D. Vanderbilt, N. Marzari, *Comput. Phys. Commun.* **2014**, *185*, 2309.
[69] D. M. Korotin, V. Mazurenko, V. Anisimov, S. Streltsov, *Phys. Rev. B* **2015**, *91*, 224405.
[70] S. Toth, B. Lake, *J. Phys.: Condens. Matter* **2015**, *27*, 166002.